Basic chemical compositions combination rules and quantitative criterion of red beds

Guangjun Cui [1,2], Jin Liao [2], Linghua Kong [2], Cuiying Zhou [2,*], Zhen Liu [2,*], Lei Yu [2],

Lihai Zhang [3]

[1] Institute of Estuarine and Coastal Research/Guangdong Provincial Engineering Research Center of Coasts, Islands and Reefs, School of Ocean Engineering and Technology, Sun Yat-sen University, Guangzhou 510275, China

[2] Guangdong Engineering Research Center for Major Infrastructures Safety, Sun Yat-sen University, Guangzhou, 510275, China

[3] The University of Melbourne, Melbourne VIC 3010, Australia

Correspondences *to*: Cuiying Zhou (zhoucy@mail.sysu.edu.cn), Zhen Liu (liuzh8@mail.sysu.edu.cn)

Abstract. Red beds belong to slippery formations, and their rapid identification is of great significance for major scientific and engineering issues such as geological hazard risk assessment and rapid response. Existing research often identifies red beds from a qualitative or semi quantitative perspective, resulting in slow recognition speed and inaccurate recognition results, making it difficult to quickly handle landslide geological disasters. Combined with the correlation between red beds geomorphic characteristics, mineral compositions, and chemical compositions, this study established a rapid quantitative identification criterion based on the basic chemical compositions combination rules in the red beds. By collecting chemical compositions data of rocks containing red beds, a total of 241,405 groups data were collected for qualitative and quantitative comparison between multiple sets of chemical composition combinations. The results indicate that simultaneously meeting the following chemical composition combinations can serve as a quantitative criterion for distinguishing red beds from other rocks: $SiO_2+Al_2O_3 \approx 50.7\%\sim85.0\%$, $Al_2O_3/SiO_2 \approx 0.14\sim0.41$, $FeO+Fe_2O_3 \approx 0.9\%\sim7.9\%$, $Fe_2O_3/FeO \approx 1.52\sim7.70$,

$K_2O+Na_2O \approx 1.6\%\sim6.8\%$, $Na_2O/K_2O \approx 0.02\sim0.43$, $CaO+MgO \approx 0.8\%\sim9.2\%$. By comparing the chemical composition

25 combinations of 15 kinds of rocks collected from China in this study, it is proven that the quantitative criterion proposed in this study are effective. The study results can be used for rapid identification of red beds, achieving risk assessment and rapid response of geological disasters such as landslides.

Keywords: red beds, quantitative criterion, geological disasters, rapid response, chemical compositions

30 **1 Introduction**

Red beds are widely distributed throughout the world (Zhou et al., 2023b; Yan et al., 2019; Chen et al., 2021). Geological disasters occur frequently in the red beds distribution area, especially landslides, debris flows, collapses, and underground engineering damage (Chen et al., 2014; Zhou et al., 2023a; Wang et al., 2022b). According to the characteristics of disasters such as landslides, the red beds belong to "landslide prone strata", and the instability of slopes with weak interlayers of the

35 red beds is particularly evident (Zhang et al., 2015). This is mainly due to the strong hydrophilicity and weak permeability of the red beds, which are prone to softening and plastic deformation under the action of water; After absorbing water, the red beds are easy to expand, and after losing water, they are easy to contract; The weathering resistance of the red beds are weak, they are easy to collapse, and their compressive and shear strength are low (Zhang et al., 2016; Wu et al., 2018; Wang et al., 2017; Marat et al., 2022; Zhang et al., 2024). The red beds have different lithology or poor binding force with other rock

40 strata, which can easily cause differential deformation and lead to rock mass sliding along the bedding plane (Liu et al., 2020; He et al., 2023; Wang et al., 2024). Therefore, the identification of rock types, especially the rapid determination of red beds, is of great significance for major scientific and engineering issues such as risk assessment and rapid response of geological disasters in red beds distribution area.

At present, the studies on red beds identification are mostly carried out from the perspectives of geomorphic

45 characteristics, mineral compositions, and chemical compositions (Cui et al., 2022; Zhou et al., 2021). And, there is a close relationship between these perspectives (Moonjun et al., 2017; Bankole et al., 2016; Perri et al., 2013). For example, the content of Fe_2O_3 or hematite in the red beds is higher than that in the grey beds (Hu et al., 2006). Among these perspectives, the research of geomorphic characteristics and mineral compositions mostly adopts qualitative or semi quantitative methods,

and there are many such studies. For example, Rainoldi et al. (2015) identified red beds by studying the color of geomorphic characteristics and hematite in mineral compositions, and studied the mechanism of red beds bleaching. Uchida et al. (2000) distinguished red sandstone, yellowish brown sandstone, and green sandstone according to the content of hematite, goethite, biotite, and muscovite in the mineral compositions, analyzed the characteristics of different rocks and pointedly protected Angkor monuments. Xue et al. (2023) distinguished red mudstone and red sandstone by quantifying the clay mineral content in the mineral compositions, in order to analyze the mechanisms and control factors of summer uplift of high-speed railway cutting. At this stage, the research on the geomorphology, mineral color and clay content of the red beds lays the foundation for the identification of the red beds, but this identification is still vague and needs to be further quantified. Therefore, some scholars have conducted quantitative studies on the chemical compositions of red beds. Hong et al. (2009) analyzed the alteration of clay minerals by studying the changes in the SiO_2/Al_2O_3 ratio in the chemical compositions of the red beds, thereby obtaining the weathering degree of the red beds. Bankole et al. (2016) studied the relationship between Fe/Mg ratio, Fe^{3+}/FeT ratio, and Cr/Fe ratio of red beds to indirectly study the oxygen content of the Paleoproterozoic. Hu et al. (2006) studied the characteristics of high Fe_2O_3 content and low FeO content in the oceanic red beds, and analyzed ancient landslides on the continental margin from the perspective of petrology. However, these studies do not distinguish between red beds and other rocks in terms of chemical compositions. The use of portable spectrometers and drone-borne multi-sensor remote sensing technique can quickly obtain the chemical compositions of rocks in geological disasters while ensuring safety (Triantafyllou et al., 2021; Kirsch et al., 2018), making it feasible to use chemical compositions as the standards to distinguish red beds from other rocks.

Therefore, the purpose of this study to develop a quantitative criterion for quickly and accurately identifying the red beds. This study first collected the data about the geomorphic characteristics, mineral content, and chemical composition of red beds and other rocks, then compared these data to obtain the basic characteristics of red beds, and finally summarized and analyzed the red beds identification criterion and verified the reliability of this criterion.

2 Methods

Figure 1 shows the methodology used in this study involving the investigation of geomorphic characteristics, mineral

compositions, and chemical compositions (the perspective of chemical compositions is the focus of this study). In this study,

75   data on geomorphological features, mineral content and chemical composition of the red beds and other rocks were first

collected, then these data were compared to derive the basic characteristics of the red beds, and finally the red bed

identification criteria were summarized and analyzed, and the reliability of the criteria was verified.
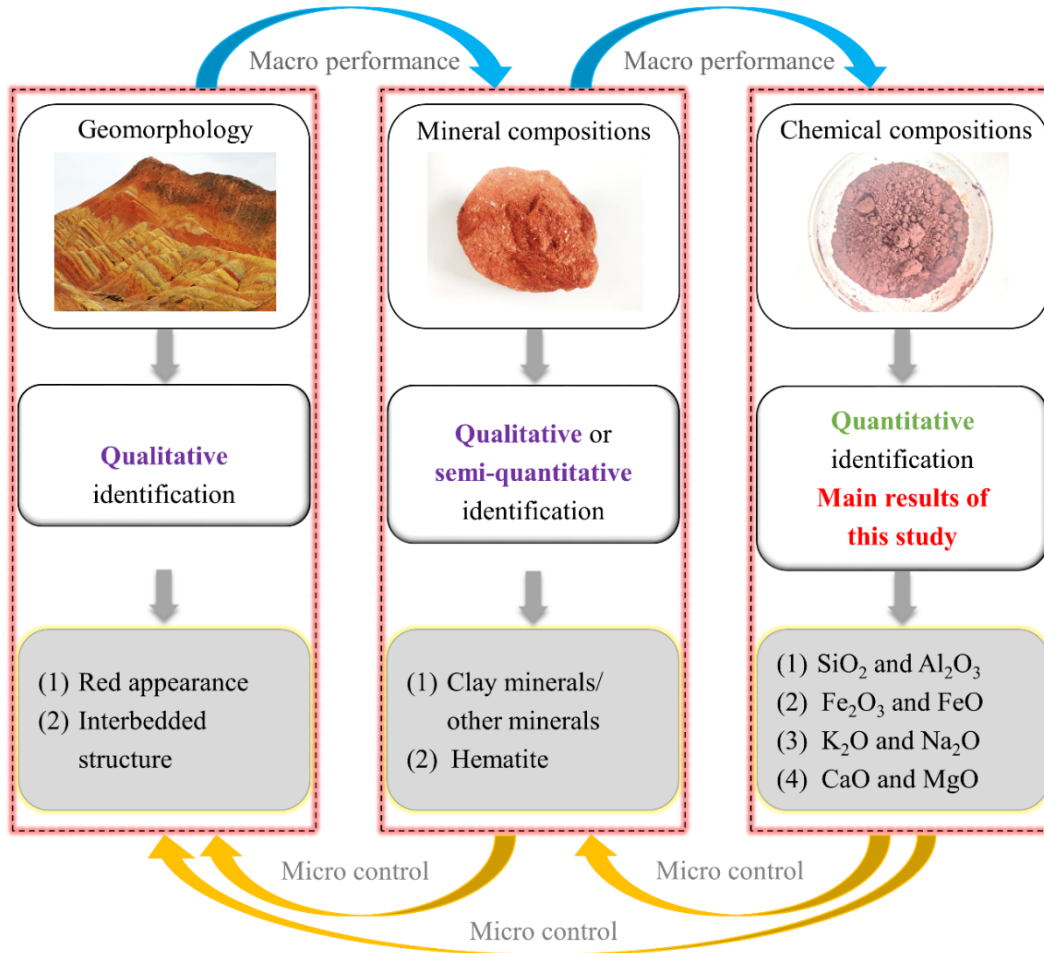
Figure 1: Methodology for identifying red beds from geomorphic characteristics, mineral compositions, and chemical

80   **compositions.**

2.1 Data collection

The geomorphic characteristics data were collected from the previous studies about landslides, debris flows, and collapses on

of red beds, igneous rocks (andesite, basalt, diorite, granite), metamorphic rocks (gneiss, marble), and other sedimentary rocks (arkose, black-shale, breccia, claystone, dolomite, lignite, limestone, marl, mudstone, siliciclastic, tuff) (e.g., (Zhang et al., 2015; San et al., 2020; He et al., 2021; Ciftci et al., 2008; Perez-Rey et al., 2019; Anbarasu et al., 2010; Xia et al., 2019; Gokbulak and Ozcan, 2008; Li et al., 2016; Wang et al., 2022a; Zhang et al., 2017; Underwood et al., 2016; Kavvadas et al., 2020; Harp et al., 2011; De Montety et al., 2007; Contino et al., 2017; Liu et al., 2018; Ni et al., 2015; Hale et al., 2021)). The geomorphic characteristics of red beds investigated in this study involve the evolution process and distribution of red beds on Earth's surface, and the results were compared with that of other types of rock samples.

The mineral compositions of red beds (1,536 groups data) were collected from the previous studies as shown in Supplementary Table 1 (e.g., (Jian et al., 2009; Liu et al., 2020; Zha et al., 2022; Bai et al., 2020; Zhang et al., 2021; Zhang et al., 2020; Yao et al., 2016; Li et al., 2023; Marat et al., 2022; Wang et al., 2017; Chen et al., 2014; Zhang et al., 2016; Li et al., 2015; Li et al., 2013; Wang et al., 2018; Wang et al., 2014)). These studies used semi quantitative or quantitative methods in XRD technology to statistically analyze the differences in mineral composition between different red beds (*e.g.,* quartz, feldspar, mica, hematite, clay minerals, and calcite), as detailed in the aforementioned literatures. This study mainly focuses on the influence of mineral compositions on geomorphic characteristics, particularly the layered structure and color of red beds.

The chemical compositions of red beds (1536 groups data) with different geological ages and various lithologies such as conglomerate, sandy conglomerate, sandstone, siltstone, shale and mudstone were collected from the previous studies as shown in Supplementary Table 2 (e.g., (Uchida et al., 2000; Xue et al., 2023; Jiang et al., 2022; Yang et al., 2016; Liu et al., 2020; Kong et al., 2018; Zhao et al., 2005; Gao et al., 2017; Zhang et al., 2008; Liu et al., 2006; Zhu et al., 2003; Liu et al., 2007; Hong et al., 2009; Wild et al., 2017)). The chemical compositions of igneous rocks, including andesite (Supplementary Table 3 - 49,203 groups data. Data were downloaded from the GEOROC database (https://georoc.mpch-mainz.gwdg.de//georoc/) on 11 May 2023, using the following parameters: search = andesite), basalt (Supplementary Table 4 - 80,365 groups data. Data were downloaded from the GEOROC database on 11 May 2023, using the following parameters: search = basalt), diorite (Supplementary Table 5 - 4,941 groups data. Data were downloaded from the GEOROC database on 11 May 2023, using the following parameters: search = diorite), and granite (Supplementary Table 6 - 17,272 groups data.

Data were downloaded from the GEOROC database on 11 May 2023, using the following parameters: search = granite). The chemical compositions of metamorphic rocks, including gneiss (Supplementary Table 7 - 24,300 groups data. The data were downloaded from the EarthChem Portal Database (http://portal.earthchem.org/) on 20 April, 2018, using the following parameters: material = metamorphic and rock name = gneiss) and marble (Supplementary Table 8 - 3,364 groups data. The data were downloaded from the EarthChem Portal Database on 12 May, 2023, using the following parameters: material = metamorphic and rock name = marble). The chemical compositions of other sedimentary rocks, including arkose (Supplementary Table 9 - 682 groups data. The data were downloaded from the EarthChem Portal Database on 10 May, 2023, using the following parameters: material = sedimentary and rock name = arkose), black-shale (Supplementary Table 10 - 305 groups data. The data were downloaded from the EarthChem Portal Database on 10 May, 2023, using the following parameters: material = sedimentary and rock name = black-shale), breccia (Supplementary Table 11 - 1,396 groups data. The data were downloaded from the EarthChem Portal Database on 10 May, 2023, using the following parameters: material = sedimentary and rock name = breccia), claystone (Supplementary Table 12 - 3,790 groups data. The data were downloaded from the EarthChem Portal Database on 10 May, 2023, using the following parameters: material = sedimentary and rock name = claystone), dolomite (Supplementary Table 13 - 2,169 groups data. The data were downloaded from the EarthChem Portal Database on 6 May, 2023, using the following parameters: material = sedimentary and rock name = dolomite), lignite (Supplementary Table 14 - 3 groups data. The data were downloaded from the EarthChem Portal Database on 24 April, 2018, using the following parameters: material = sedimentary and rock name = lignite), limestone (Supplementary Table 15 - 9,104 groups data. The data were downloaded from the EarthChem Portal Database on 10 May, 2023, using the following parameters: material = sedimentary and rock name = limestone), marl (Supplementary Table 16 - 142 groups data. The data were downloaded from the EarthChem Portal Database on 10 May, 2023, using the following parameters: material = sedimentary and rock name = marlstone, marl), mudstone (Supplementary Table 17 - 6,140 groups data. The data were downloaded from the EarthChem Portal Database on 10 May, 2023, using the following parameters: material = sedimentary and rock name = mudstone, mud), siliciclastic (Supplementary Table 18 - 26,938 groups data. The data were downloaded from the EarthChem Portal Database on 10 May, 2023, using the following parameters: material = sedimentary and rock name = siliciclastic), tuff (Supplementary Table 19 - 10,295 groups data. The data were downloaded from the EarthChem

Portal Database on 6 May, 2023, using the following parameters: material = sedimentary and rock name = tuff). Due to the high content of quartz, clay minerals, hematite, calcite, dolomite, feldspar, etc. in the red beds, the main oxide components are SiO_2, Al_2O_3, Fe_2O_3, FeO, CaO, MgO, Na_2O, and K_2O, this study mainly focuses on the differences in chemical compositions combination rules between the red beds and other rocks, such as SiO_2 and Al_2O_3, Fe_2O_3 and FeO, CaO and MgO, Na_2O and K_2O.

2.2 Criterion verification

In order to verify the proposed basic chemical compositions combination rules and quantitative criterion of red beds, 15 kinds of rocks of known rock types were selected in Guangdong, Sichuan, Hubei, Zhejiang, and Anhui provinces (Figure 2), including 12 kinds of red beds (red claystone, red mudtone, red silty mudstone, red argillaceous siltstone, red fine sandstone, red medium sandstone, red coarse sandstone, red conglomerate, etc.), limestone (1 kind), arkose (1 kind) and mudstone (1 kind). After on-site sampling, use a hammer to smash the rock block out of the fresh surface. Then, the fresh surface was analyzed using the MiX5 Pro handheld X-ray fluorescence element analyzer (Figure 3) from Sun Yat-sen University to check whether these elements conform to the basic chemical compositions combination rules of red beds proposed by this study.
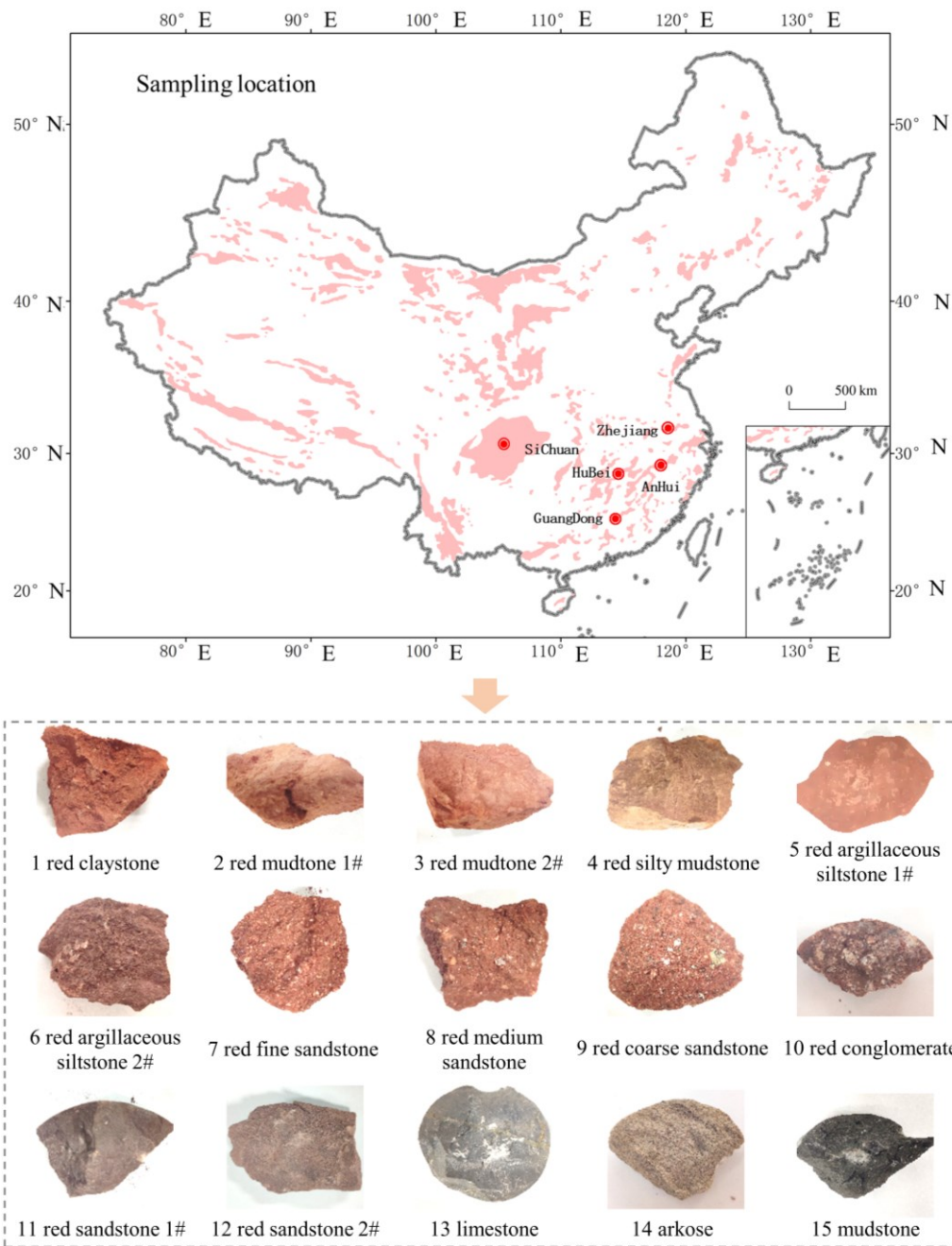
Figure 2: Distribution areas of red beds in China and sampling locations for 15 types of rocks.

The working principle of the element analyzer is that a miniature X-ray source provides tube voltage and tube current,

and the light tube emits continuous X-ray spectral lines. The X-rays irradiated on the sample knock out the inner electrons of the K and L layers of the element atoms, and the holes in the low-energy layer are filled by high-energy outer electrons (N

155   layer). The high-energy electrons emit excess energy as X-ray fluorescence (Kα) with elemental characteristics. Thus, the instrument detects the type and concentration of elements through the emitted spectral lines. On the instrument analysis interface, point the detection window towards the rock sample and press the trigger to start and stop the measurement. After amplification and data collection, the signal is processed to obtain the required test data. The instrument can detect elements with atomic number greater than or equal to 12, that is, element Na that cannot get the above attention (atomic number is 11).

160   Therefore, the content of Na element is determined based on the median of Na_2O/K_2O of the corresponding rock in Section 3.3 and K element detected by the MiX5 Pro handheld X-ray fluorescence element analyzer. Moreover, the Fe element content obtained by this instrument is the content of Fe_2O_3+FeO. The corresponding Fe_2O_3 and FeO contents are determined based on the median of Fe_2O_3/FeO of the corresponding rock in Section 3.3 and Fe_2O_3+FeO detected by the MiX5 Pro handheld X-ray fluorescence element analyzer.

165
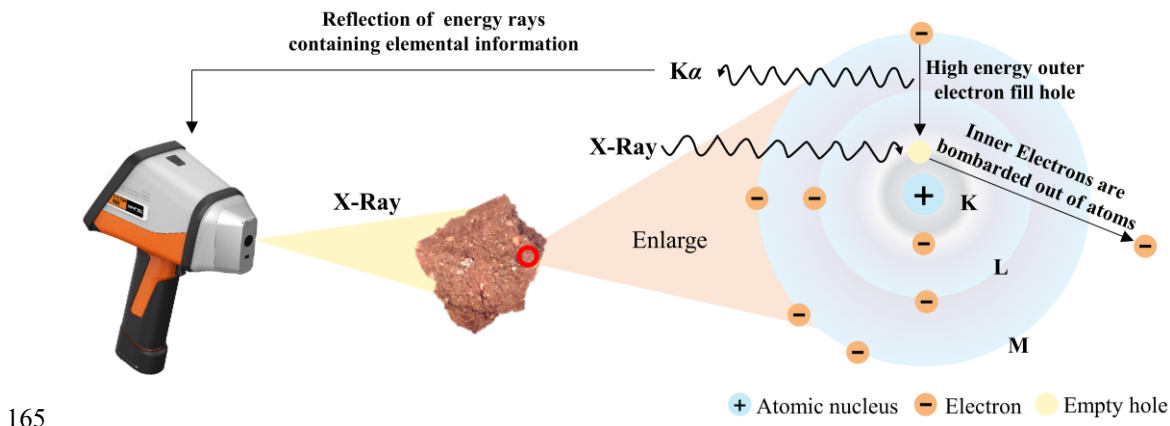
Figure 3: MiX5 Pro handheld X-ray fluorescence element analyzer.

3. Results and discussions

3.1 Geomorphic characteristics of red beds

170   Geomorphic characteristics of the red beds as shown in Figure 4. Red beds are sedimentary rocks of different geological ages (mainly Mesozoic and Cenozoic) with bedding structure typically consisting of various lithologies such as conglomerate,

sandy conglomerate, sandstone, siltstone, shale and mudstone that are predominantly red in color due to the presence of ferric oxides (Yan et al., 2019). Owing to differences in depositional environments and influences of late stage geologic processes, the color of red beds can be brownish-reddish-yellow, brownish-yellow, purplish-red, brownish-red, grayish-purple and other reddish tints (Yan et al., 2019; Nance, 2015), making it difficult to accurately describe using the CIELAB color space and/or Munsell color system. Bedding is a common structural feature of sedimentary rocks representing the changes in the sedimentary environment. The sandstone is one of the most common types of red beds, with a distinct reddish appearance. Compared with the obvious layering and red appearance characteristics of red beds, igneous rocks and metamorphic rocks do not show the two characteristics of red appearance and bedding at the same time. Basalts are reddish in appearance but does not have bedding (Cunha et al., 2005). In addition, andesites are mainly light black and have a columnar structure which is similar to that of basalts (Feizizadeh et al., 2021). Most of granites are grey or light brown with a significantly different structure compared to red beds (Migon et al., 2018), while gneisses are generally characterized as a dark and light gneissic structure (Garajeh et al., 2022). Although the red color appearance and bedding structure can be used as qualitative criteria for identifying the red beds, the analysis of mineral and chemical compositions is still necessary for identifying the rocks from quantitative perspective.

Red beds Yadan landform   Red beds Danxia landform

Figure 4: Geomorphic characteristics of the red beds.

3.2 Mineral compositions of red beds

Table 1 shows the statistical analysis results of mineral compositions of red beds in Supplementary Table 1. The common minerals in the red bed are quartz (median value is 40%, the same below), clay minerals (35%, including kaolinite, illite,

montmorillonite, and chlorite), feldspar (10%, including K-feldspar and plagioclase), calcite (10%), mica (7%, including biotite, muscovite and sericite), and hematite (3%) according to their content. According to the average value and standard deviation, it can be seen that the content range of various minerals has significant dispersion. The ratio of the content of clay minerals to other minerals (quartz, feldspar, mica, hematite, and calcite) ranges between 0.11 to 1.50. The hematite content ranges between 1.5% and 10.0% (percentile=10%~90%), and reddish appearance of red beds is due to the abundant hematite content of the rocks. The change in mineral compositions of red beds could lead to the change in rock color which is one of the major characteristics of red beds. Furthermore, when the red beds encounter water, softening and expansion could happen because of the large amount of clay minerals in the rocks, especially the mudstone. The differences in mineral compositions of the red beds can also be quantitatively described through their chemical composition combination characteristics (Table 2).

Table 1: Mineral compositions of red beds.

Minerals	Range (per = 0%~100%)	Range (per = 10%~90%)	Median value (per = 50%)	Average value	Standard deviation
Quartz (%)	2.3~94.0	21.0~69.0	40.0	42.6	18.8
Clay minerals (%)	1.0~80.0	7.8~59.0	35.0	34.1	18.6
Feldspar (%)	0.4~71.0	2.3~25.0	10.0	12.6	10.7
Mica (%)	0.1~40.8	3.0~20.0	7.0	9.2	8.2
Hematite (%)	0.4~25.2	1.5~10.0	3.0	5.0	4.4
Calcite (%)	0.7~97.7	3.1~23.5	10.0	12.2	10.0
Clay minerals/ Other minerals	0.01~6.00	0.11~1.50	0.61	0.76	0.66

Note: per – percentile; Other minerals – quartz, feldspar, mica, hematite, and calcite.

Table 2: Chemical composition of minerals in red beds (%).

Mineral chemical formulas	SiO_2	Al_2O_3	Fe_2O_3	FeO	CaO	MgO	Na_2O	K_2O	H_2O	CO_2
Quartz (SiO_2)	100.0									
Potassium feldspar ($KAlSi_3O_8$)	64.7	18.4						16.9		
Sodium feldspar ($NaAlSi_3O_8$)	68.8	19.4					11.8			
Calcium feldspar ($CaAl2Si_2O_8$)	43.2	36.7			20.1					
White mica ($KAl_2(AlSi_3O_{10})(OH,F)_2$)	45.2	38.4						11.8	4.1	
Biotite ($KMg_3[Si_3 AlO_{10}](OH,F)_2$)	43.0	12.2				28.8		11.2	2.2	

Mineral									
Phlogopite ($K(Mg,Fe)_3AlSi_3O_{10}(F,OH)_2$)	41.6	11.8		8.3		23.2	0.5	10.9	3.6
Hematite (Fe_2O_3)			100.0						
Calcite ($CaCO_3$)					56.0				44.0
Kaolinite ($Al_2Si_2O_5(OH)_4$)	46.6	39.5							14.0
Illite ($K_{0.75}(Al_{1.75}R)[Si_{3.5}Al_{0.5}O_{10}](OH)_2$)	54.0	17.0		1.9		3.1		7.3	12.0
Montmorillonite ($(Na,Ca)_{0.33}(Al,Mg)_2[Si4O_{10}](OH)_2 \cdot nH_2O$)	43.8	18.6			1.0		1.1		36.1
Chlorite ($Y_3[Z_4O_{10}](OH)_2 \cdot Y_3(OH)_6$)	30.3	17.1		15.1		25.4			12.1

205   Note: Data collected from http://webmineral.com/ and https://www.mindat.org/.

3.3 Chemical composition characteristics of red beds

Figures 5~6 are mainly used to qualitatively analyze the differences in chemical compositions between the red beds and other rocks through scatter plots. The area surrounded by black dashed lines is the area where the red beds data points are

210   located. To better distinguish various rock data points, the distribution areas of various rock data are shown on the right side of the figure, and the corresponding colored dashed ellipses are used to indicate the distribution areas in the dataset. Figure 4 shows the comparison of SiO_2 and Al_2O_3, FeO and Fe_2O_3, K_2O and Na_2O, CaO and MgO contents in red beds, igneous rocks, and metamorphic rocks, respectively. Figure 5 shows the comparison of SiO_2 and Al_2O_3, FeO and Fe_2O_3, K_2O and Na_2O, CaO and MgO contents in red beds and other sedimentary rocks respectively.

215   The content of SiO_2 in the red beds is about 30%~80%, Al_2O_3 is about 8%~30%, Fe_2O_3 is about 0%~10%, FeO is about 0%~3%, K_2O is about 0%~10%, Na_2O is about 0%~2.5%, CaO is about 0%~10%, and MgO is about 0%~5%. Compared with igneous rocks, metamorphic rocks, and other sedimentary rocks, the content of each chemical composition of the red beds has three relationships with the content of corresponding chemical composition of other rocks: inclusion relationship (the data distribution range of one rock completely covers and is larger than the data range of the other rock), intersection

220   relationship (the data distribution range of one rock intersects with the data distribution range of another rock), and mutual difference relationship (the data distribution range of one rock does not intersect at all with the data distribution range of another rock). The distribution range of SiO_2 and Al_2O_3 content in the red beds includes the distribution range of SiO_2 and Al_2O_3 content in 9 types of rocks, namely andesite, basalt, diorite, granite, black shale, claystone, mudstone, siliciclastic, and tuff. The distribution range of SiO_2 and Al_2O_3 content in the red beds intersects with that in breccia, lignite, and marl. The

225 distribution range of SiO_2 and Al_2O_3 content in gneiss, marble, arkose, dolomite, and limestone is different from that in the red beds. The distribution range of Fe_2O_3 and FeO content in the red beds includes the distribution range of Fe_2O_3 and FeO content in granite, marble, and lignite. The distribution range of Fe_2O_3 and FeO content in the red beds intersects with that in 8 kinds of rocks, namely, andesite, basalt, diorite, breccia, claystone, dolomite, limestone, and mudstone. The distribution range of Fe_2O_3 and FeO content in gneiss, arkose, black shale, siliciclastic, and tuff is different from that in the red beds. The

230 distribution range of K_2O and Na_2O content in the red beds includes the distribution range of K_2O and Na_2O content in lignite. The distribution range of K_2O and Na_2O content in the red beds intersects with that in 15 kinds of rocks, including andesite, basalt, diorite, granite, marble, arkose, black shale, breccia, claystone, dolomite, limestone, marl, mudstone, siliciclastic, and tuff. The distribution range of K_2O and Na_2O content in gneiss is different from that in the red beds. The distribution range of CaO and MgO content in the red beds includes the distribution range of CaO and MgO content in

235 granite, black shale, and lignite. The distribution range of CaO and MgO content in the red beds intersects with that in 13 types of rocks, including andesite, basalt, diorite, gneiss, arkose, breccia, claystone, dolomite, limestone, marl, mudstone, siliciclastic, and tuff. The distribution range of CaO and MgO content in marble is different from that in the red beds. Therefore, from a qualitative perspective, it can be seen that the red beds differ in chemical composition from 8 kinds of rocks, including gneiss, marble, arkose, dolomite, limestone, black-shale, siliciclastic, and tuff, and also intersects with other

240 rocks to varying degrees. But this is not enough as a criterion to determine the difference between red beds and other rocks.
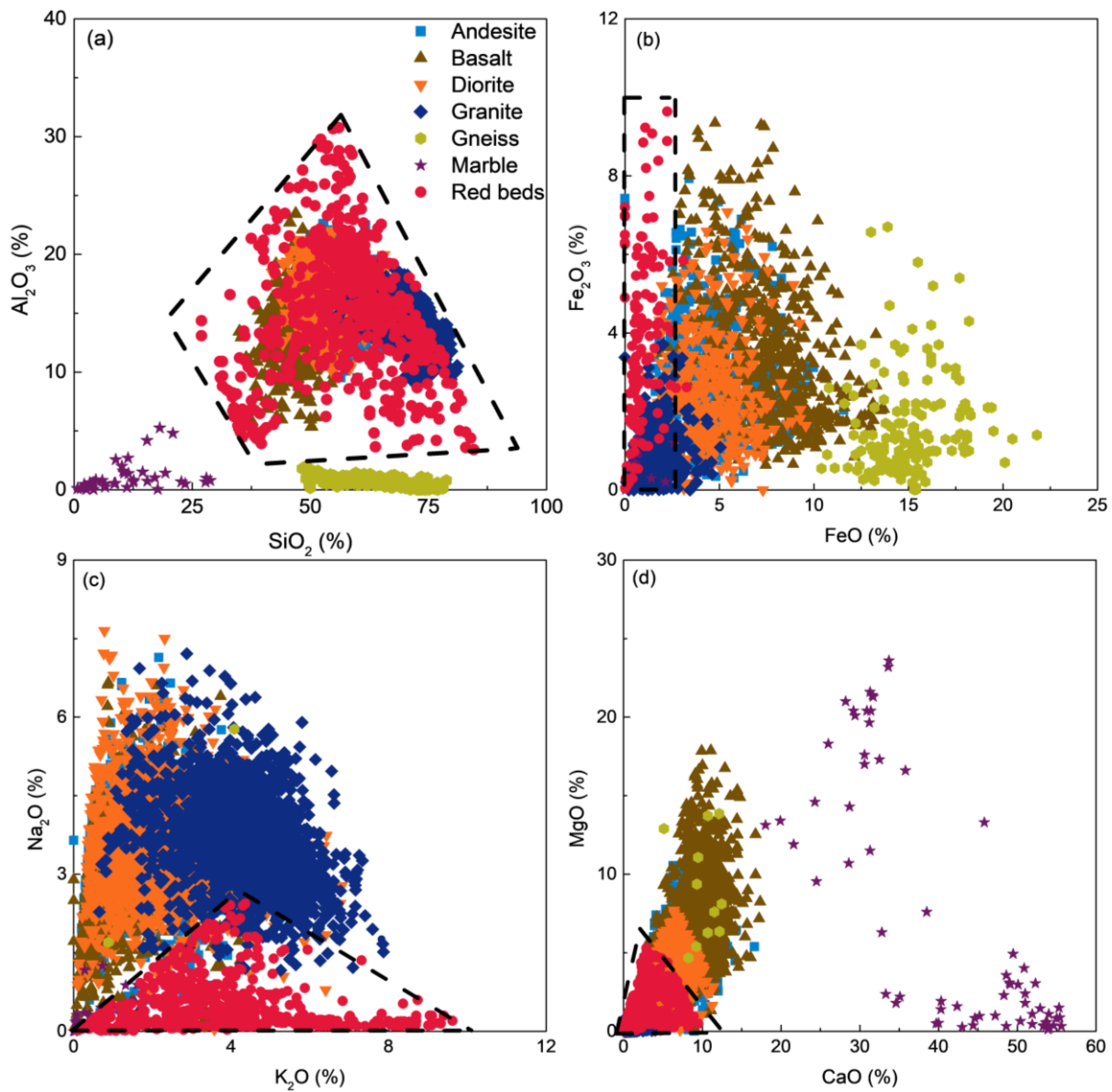
Figure 5: Comparison of (a) SiO₂ and Al₂O₃, (b) FeO and Fe₂O₃, (c) K₂O and Na₂O, (d) CaO and MgO contents in red beds, igneous rock, and metamorphic rocks, respectively (Note: Icons of the same color in the figure have the same meanings).
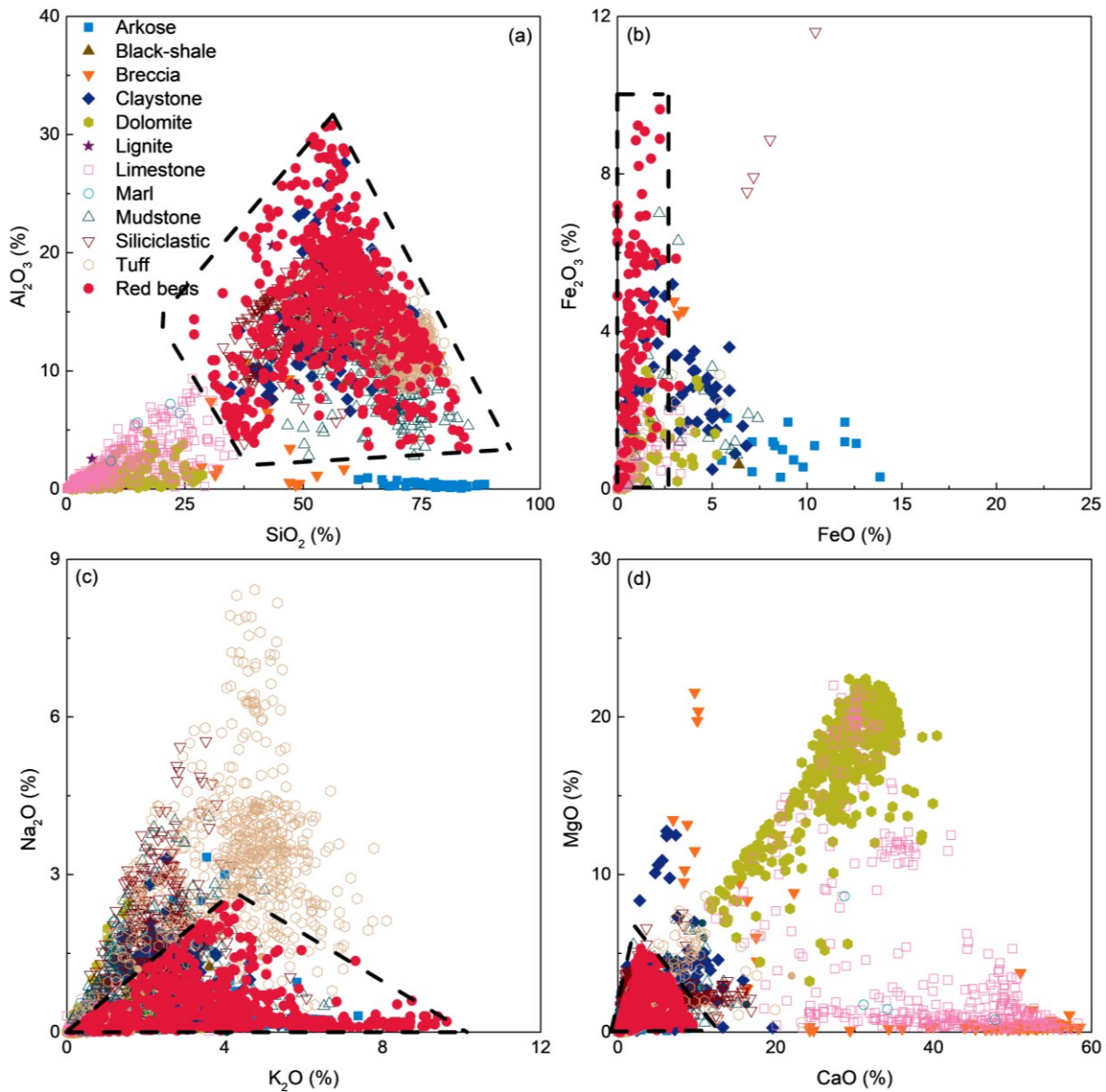
Figure 6: Comparison of (a) SiO$_2$ and Al$_2$O$_3$, (b) FeO and Fe$_2$O$_3$, (c) K$_2$O and Na$_2$O, (d) CaO and MgO contents in red beds and other sedimentary rocks respectively (Note: Icons of the same color in the figure have the same meanings).

Figures 7~8 mainly analyze the differences in chemical compositions between red beds and other rocks through further data statistics and box plots of the scatter plots mentioned above, and propose quantitative identification criterion for the red beds chemical compositions combination. The red dashed box in the figure represents rocks that differ from the red beds data,

while the black dashed box represents rocks that intersect less than 25% with the red beds data. The data collected in section 2.1 comes from published papers or databases, and its accuracy and robustness have been explained in relevant literature. In order to ensure the exclusion of outliers in the box plots mentioned above during the analysis of this study. The horizontal gray dashes corresponding to the red beds box chart represent 10% percentile (the same below), lower quartile (25% percentile), median (50% percentile), upper quartile (75% percentile), and 90% percentile in the red beds data from bottom to top. Figure 6 shows the chemical compositions combination comparison of $SiO_2+Al_2O_3$ (total content, the same below) and Al_2O_3/SiO_2 (content ratio, the same below), $FeO+Fe_2O_3$ and Fe_2O_3/FeO, K_2O+Na_2O and Na_2O/K_2O, $CaO+MgO$ and MgO/CaO in red beds, igneous rock, and metamorphic rocks, respectively. Figure 7 respectively shows the chemical compositions combination comparison of $SiO_2+Al_2O_3$ and Al_2O_3/SiO_2, $FeO+Fe_2O_3$ and Fe_2O_3/FeO, K_2O+Na_2O and Na_2O/K_2O, $CaO+MgO$ and MgO/CaO in red beds and other sedimentary rocks.

The $SiO_2+Al_2O_3$ content in the red beds is 54.7%~85.0% (10%~90% percentile, the same below), the Al_2O_3/SiO_2 ratio is 0.14~0.41, the $FeO+Fe_2O_3$ content is 0.9%~7.9%, the Fe_2O_3/FeO ratio is 1.52~7.70, the K_2O+Na_2O content is 1.6%~6.8%, the Na_2O/K_2O ratio is 0.02~0.43, the $CaO+MgO$ content is 0.8%~9.2%, and the MgO/CaO ratio is 0.16~1.57. By comparing the content of $SiO_2+Al_2O_3$, the red beds are distinct or have small intersections (less than 25%, the same below) with granite, marble, dolomite, lignite, limestone, and marl. By comparing the Al_2O_3/SiO_2 ratio, it is found that the red beds are distinct or have small intersections with gneiss, marble, arkose, and lignite. By comparing the content of $FeO+Fe_2O_3$, it is found that the red beds are distinct or have small intersections with basalt, gneiss, arkose, and siliciclastic. By comparing the Fe_2O_3/FeO ratio, it is found that the red beds are distinct or have small intersections with andesite, basalt, diorite, granite, gneiss, marble, arkose, black shale, dolomite, mudstone, siliclastic, and tuff. Through the comparison of K_2O+Na_2O content, the red beds are distinct or have small intersections with granite, marble, breccia, dolomite, and limestone. By comparing the Na_2O/K_2O ratio, the red beds are distinct or have small intersections with andesite, basalt, diorite, gneiss, lignite, siliciclastic, and tuff. Through the comparison of $CaO+MgO$ content, the red beds are distinct or have small intersections with andesite, basalt, gneiss, marble, breccia, dolomite, limestone, and marl. By comparing the MgO/CaO ratio, it is difficult to distinguish the red beds from other rocks.

275
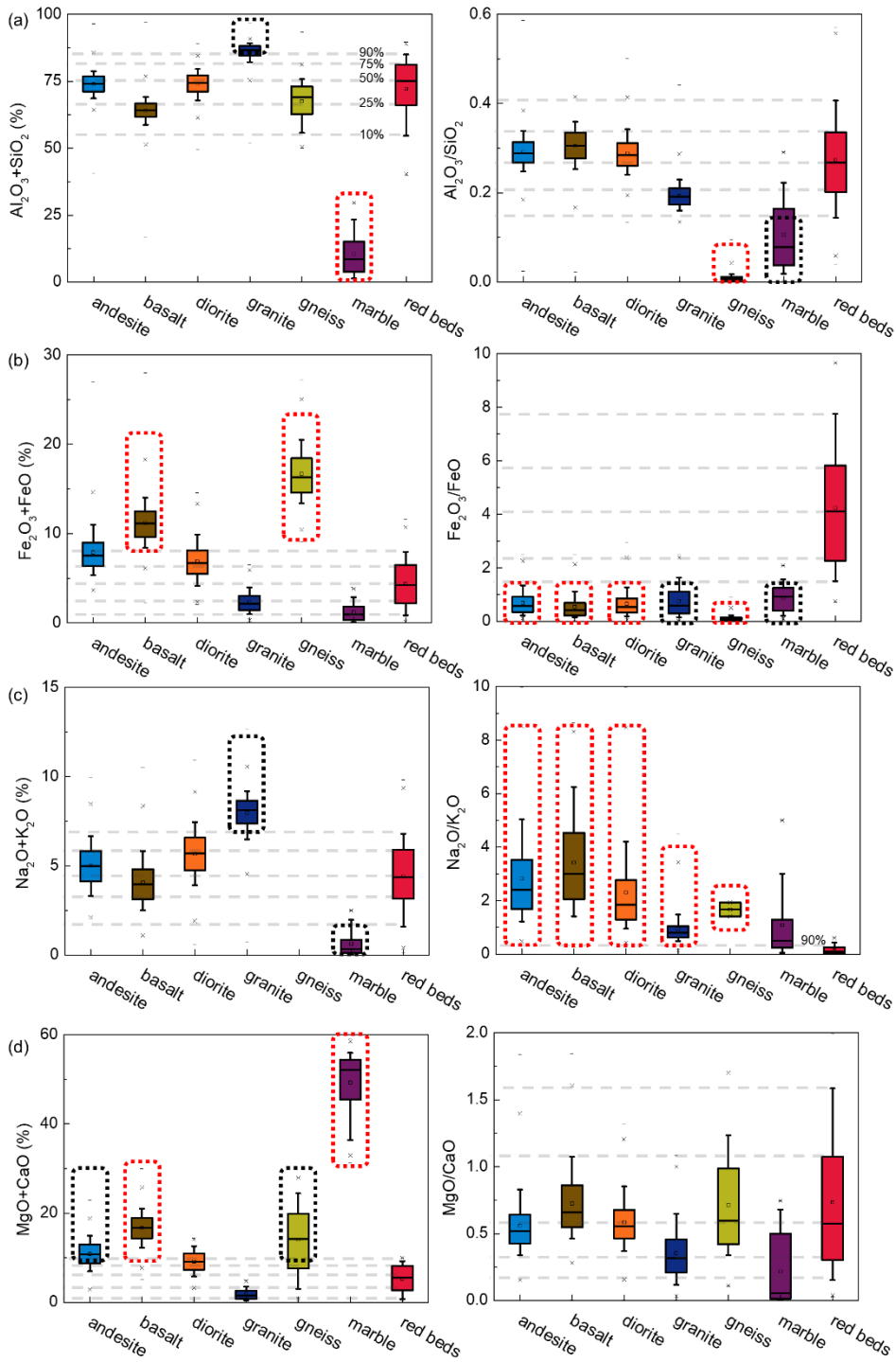
Figure 7: Chemical compositions comparison of (a) SiO$_2$+Al$_2$O$_3$, Al$_2$O$_3$/SiO$_2$, (b) FeO+Fe$_2$O$_3$, Fe$_2$O$_3$/FeO, (c) K$_2$O+Na$_2$O, Na$_2$O/K$_2$O, (d) CaO+MgO, MgO/CaO in red beds, igneous rock, and metamorphic rocks.
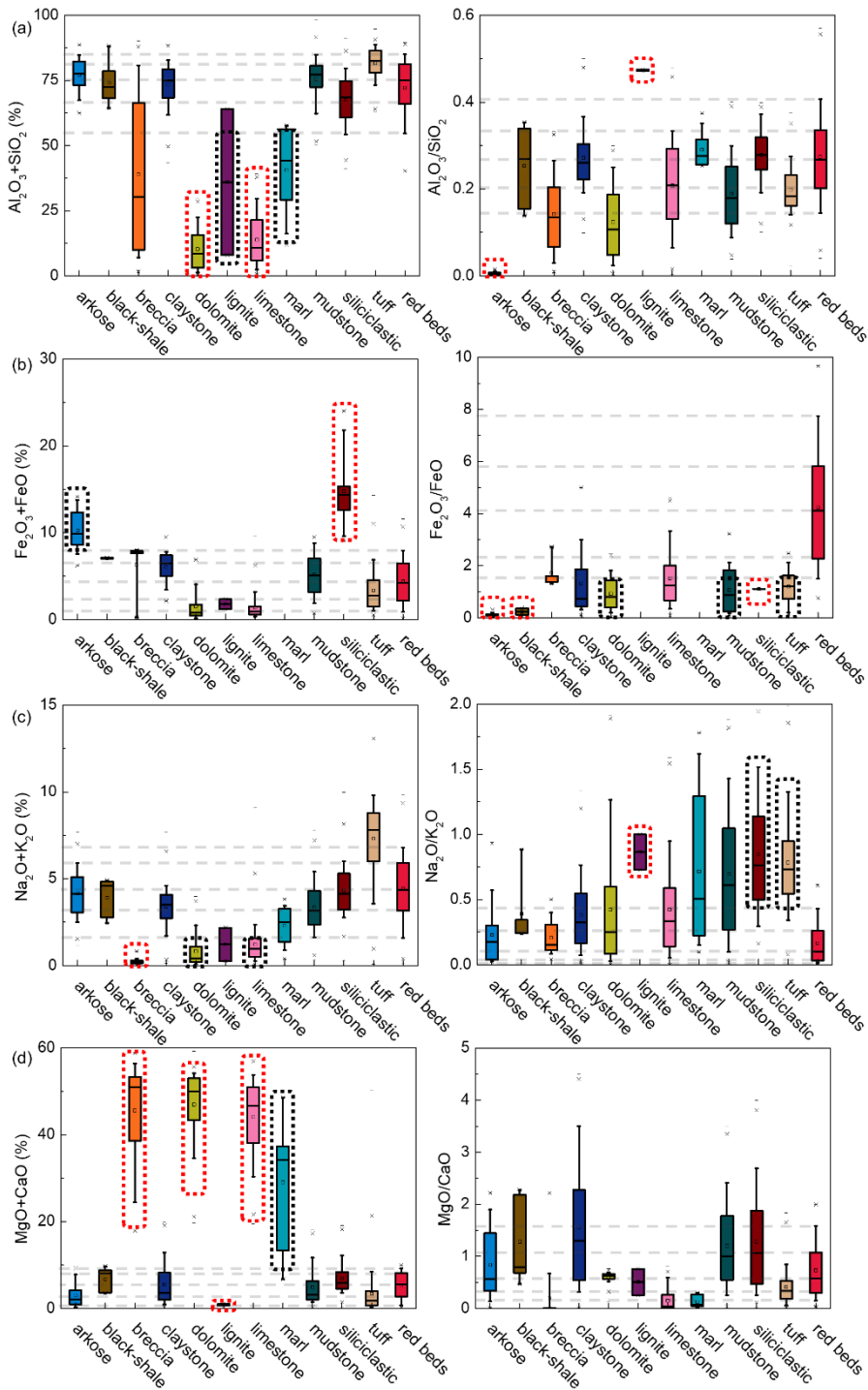
Figure 8: Chemical compositions comparison of (a) SiO₂+Al₂O₃, Al₂O₃/SiO₂, (b) FeO+Fe₂O₃, Fe₂O₃/FeO, (c) K₂O+Na₂O, Na₂O/K₂O, (d) CaO+MgO, MgO/CaO in red beds and other sedimentary rocks.

In summary, there are differences in chemical compositions between red beds and other rocks, and the use of chemical compositions combination rules can serve as a quantitative criterion for identifying red beds. Simultaneously meeting the following chemical compositions combinations as a quantitative criterion to distinguish red beds with different geological ages and various lithologies from other rocks: $SiO_2+Al_2O_3 \approx 50.7\%\sim85.0\%$, $Al_2O_3/SiO_2 \approx 0.14\sim0.41$, $FeO+Fe_2O_3 \approx 0.9\%\sim7.9\%$, $Fe_2O_3/FeO \approx 1.52\sim7.70$, $K_2O+Na_2O \approx 1.6\%\sim6.8\%$, $Na_2O/K_2O \approx 0.02\sim0.43$, $CaO+MgO \approx 0.8\%\sim9.2\%$.

3.4 Red beds identification quantization criterion verification

The chemical composition combinations of the 15 selected rocks in this study are shown in Table 3. The chemical composition combinations of 12 kinds of red beds are all within the scope of the quantitative criterion (Figure 10). There are some chemical composition combinations of the 3 non-red beds sedimentary rocks (limestone, arkose, and mudstone) that are outside the scope of the red beds quantitative criterion (the numbers in bold and underlined in the table). For example, the content of $SiO_2+Al_2O_3$, $FeO+Fe_2O_3$, K_2O+Na_2O in limestone is lower than the range of quantification criterion, while the content of $CaO+MgO$ in limestone is higher than the range of quantification criterion; Fe_2O_3/FeO and K_2O+Na_2O in arkose are below the quantification criterion; $SiO_2+Al_2O_3$ and Na_2O/K_2O in mudstone are higher than the quantification criterion, while Fe_2O_3/FeO and K_2O+Na_2O are lower than the quantification criterion. This is consistent with the research results in Figure 9, once again proving the reliability of the quantification criterion proposed in this study.

Table 3: Chemical composition combinations of 15 kinds of rocks.

No.	SiO_2 (%)	Al_2O_3 (%)	Fe_2O_3 (%)	FeO (%)	Na_2O (%)	K_2O (%)	MgO (%)	CaO (%)	SiO_2+ Al_2O_3 (%)	$Al_2O_3/$ SiO_2	$FeO+$ Fe_2O_3 (%)	$Fe_2O_3/$ FeO	K_2O+ Na_2O (%)	$Na_2O/$ K_2O	$CaO+$ MgO (%)
1	43.3	15.0	2.9	0.7	0.2	1.9	3.3	1.1	58.3	0.35	3.6	4.12	2.1	0.10	4.4
2	45.8	18.3	4.1	1.0	0.3	2.6	2.3	0.0	64.1	0.40	5.1	4.12	2.9	0.10	2.3
3	40.1	15.5	3.7	0.9	0.2	2.1	3.6	0.0	55.6	0.39	4.6	4.12	2.3	0.10	3.6
4	48.8	14.3	3.1	0.7	0.3	2.9	2.9	6.1	63.1	0.29	3.8	4.12	3.2	0.10	9.0
5	62.0	15.8	2.7	0.6	0.3	3.2	3.1	0.0	77.8	0.26	3.3	4.12	3.5	0.10	3.1
6	42.8	9.4	1.6	0.4	0.2	1.5	0.4	4.1	52.2	0.22	2.0	4.12	1.7	0.10	4.5

7	52.2	17.1	1.5	0.4	0.2	2.3	2.5	0.0	69.3	0.33	1.9	4.12	2.5	0.10	2.5
8	58.3	18.6	1.6	0.4	0.2	1.9	4.0	0.8	76.9	0.32	2.0	4.12	2.1	0.10	4.8
9	39.9	11.2	1.3	0.3	0.2	1.5	3.9	0.0	51.1	0.28	1.4	4.12	1.7	0.10	3.9
10	48.2	9.6	1.0	0.2	0.2	2.4	3.5	1.9	57.8	0.20	1.2	4.12	2.6	0.10	5.4
11	50.5	14.2	2.1	0.5	0.2	2.3	0.8	5.1	64.7	0.28	2.6	4.12	2.5	0.10	5.9
12	45.1	8.4	3.5	0.8	0.2	2.0	2.3	1.6	53.5	0.19	4.3	4.12	2.2	0.10	3.9
13	13.6	2.3	0.1	0.1	0.2	0.5	3.2	39.6	*15.9*	0.17	*0.2*	1.23	*0.7*	0.33	*42.8*
14	56.9	14.9	0.3	2.3	0.2	1.3	3.3	1.1	71.8	0.26	2.6	0.11	*1.5*	0.18	4.4
15	69.7	21.2	0.6	0.7	0.3	0.5	0.9	0.0	*90.9*	0.30	1.3	0.87	*0.8*	0.61	0.9

3.5 Research results application methods

Figure 10 shows the application methods of the research results. According to the methods for emergency management of landslide geological disasters (Fu et al., 2021), landslide risk assessment (including risk identification, risk analysis, and risk assessment) and risk management (developing and selecting treatment plans, as well as planning, implementing, and evaluating treatment methods) need to be carried out before the landslide occurs. In the field of engineering geology, risk identification is the most important prerequisite for landslide emergency response. Red beds is the slippery layer that needs to be identified in risk identification.
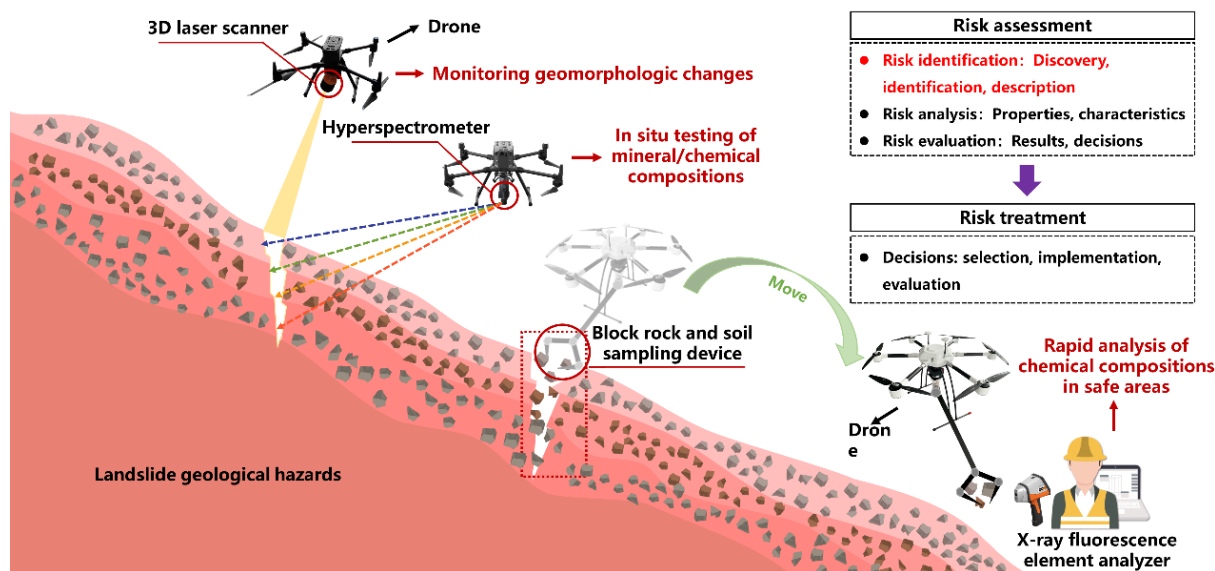
Figure 10: Research results used for risk identification.

310   At present, the commonly used risk identification method is to use drones to carry image capture devices for three-dimensional reconstruction of slope images, determine the volume of landslide accumulation, and determine the shape changes of the slope (Chen et al., 2020; Fu et al., 2021), which can be also used for mountain rescue (Wankmuller et al., 2021). Based on the drone technology, combined with the Optech Polaris LR 3D laser scanner and the HY-9070 hyperspectral analyzer of Sun Yat-sen University, the landslide shape change and remote monitoring of mineral and

315   chemical compositions can be realized to identify whether it is a red beds landslide. It can also use a drone equipped with a block rock and soil sampling device to collect representative blocks of rock and soil within cracks to a safe area, and then use the MiX5 Pro handheld X-ray fluorescence element analyzer for rapid analysis. Therefore, the research results can be used for rapid identification of red beds, achieving risk assessment and rapid response of geological disasters such as landslides.

320

4. Conclusions

(1) In response to the rapid identification of red beds in geological disaster emergency response, a rapid quantitative identification criterion based on the basic chemical compositions combination rules of red beds has been established, taking into account the correlation between red beds geomorphic characteristics, mineral compositions, and chemical compositions.

325   It solves the current problem of fuzzy identification of the red beds.

(2) The results indicate that the red beds in the geomorphic characteristics have obvious interlayer characteristics and its appearance is red. In mineral composition, the ratio of clay minerals to other minerals of red beds ranges from 0.11 to 1.50, and the content of hematite of red beds ranges from 1.5% to 10.0%. The following chemical composition combinations can be used as red beds quantification criterion: $SiO_2+Al_2O_3 \approx 50.7\%\sim85.0\%$, $Al_2O_3/SiO_2 \approx 0.14\sim0.41$,

330    $FeO+Fe_2O_3 \approx 0.9\%\sim7.9\%$, $Fe_2O_3/FeO \approx 1.52\sim7.70$, $K_2O+Na_2O \approx 1.6\%\sim6.8\%$, $Na_2O/K_2O \approx 0.02\sim0.43$, $CaO+MgO \approx 0.8\%\sim9.2\%$. The reliability of the quantitative criterion was verified by collecting 15 kinds of rocks and analyzing their chemical composition combinations.

(3) The combination of research results with existing landslide geological hazard risk identification techniques can

effectively carry out rapid response to geological disasters, which is very important for emergency response to geological

335   disasters. Moreover, the research results can also be applied to the quantitative identification of red beds in other fields such

as resources, ecology, environment, energy, materials, etc.

Declarations

Availability of data and materials

340   The data that support the findings of this study are available in supplementary materials.

Competing interests

The authors declare no conflict of interest. The funders had no role in the design of the study; in the collection, analyses,

or interpretation of data; in the writing of the manuscript, or in the decision to publish the results.

Funding

345   The research is supported by the National Natural Science Foundation of China (NSFC) (Grant Numbers: 42293354,

42293351, 42293355, 42277131, 41977230, and 42293350).

Authors' contributions

Conceptualization, C.Z. and Z.L.; methodology, G.C. and Z.L.; software, G.C. and L.K.; validation, G.C., L.K., and

Z.L.; formal analysis, C.Z. and Z.L.; investigation, G.C., J.L., and L.Y.; resources, G.C. and L.K.; data curation, G.C., J.L.,

350   L.Y. and L.K.; writing—original draft preparation, G.C. and L.K.; writing—review and editing, G.C., Z.L., and L.Z.;

visualization, L.Y.; supervision, Z.L. and L.Z.; project administration, C.Z.; funding acquisition, C.Z. All authors have read

and agreed to the published version of the manuscript.

Acknowledgments

The authors would like to thank the anonymous reviewers for their very constructive and helpful comments.

355   **Supplementary Materials**

Supplementary Table 1: Mineral compositions of the red beds.

Supplementary Table 2: Chemical compositions of the red beds.

Supplementary Table 3: Chemical compositions of the andesite.

Supplementary Table 4: Chemical compositions of the basalt.

360  Supplementary Table 5: Chemical compositions of the diorite.

Supplementary Table 6: Chemical compositions of the granite.

Supplementary Table 7: Chemical compositions of the gneiss.

Supplementary Table 8: Chemical compositions of the marble.

Supplementary Table 9: Chemical compositions of the arkose.

365  Supplementary Table 10: Chemical compositions of the black-shale.

Supplementary Table 11: Chemical compositions of the breccia.

Supplementary Table 12: Chemical compositions of the claystone.

Supplementary Table 13: Chemical compositions of the dolomite.

Supplementary Table 14: Chemical compositions of the lignite.

370  Supplementary Table 15: Chemical compositions of the limestone.

Supplementary Table 16: Chemical compositions of the marl.

Supplementary Table 17: Chemical compositions of the mudstone.

Supplementary Table 18: Chemical compositions of the siliciclastic.

Supplementary Table 19: Chemical compositions of the tuff.

375

References

Anbarasu, K., Sengupta, A., Gupta, S., and Sharma, S. P.: Mechanism of activation of the Lanta Khola landslide in Sikkim Himalayas, Landslides, 7, 135-147, 10.1007/s10346-009-0193-0, 2010.

Bai, Y., Shan, R., Ju, Y., Wu, Y., Tong, X., Han, T., and Dou, H.: Experimental study on the strength, deformation and crack

380  evolution behaviour of red sandstone samples containing two ice-filled fissures under triaxial compression, Cold Regions Science and Technology, 174, 10.1016/j.coldregions.2020.103061, 2020.

Bankole, O. M., Albani, A. E., Meunier, A., Rouxel, O. J., Oisgauthier-Lafaye, F., and Bekker, A.: Origin of Red Beds in the Paleoproterozoic Franceville Basin, Gabon, and Implications for Sandstone-Hosted Uranium Mineralization, Am J Sci, 316, 839-872, 10.2475/09.2016.02, 2016.

385 Chen, J., Dai, F., Xu, L., Chen, S., Wang, P., Long, W., and Shen, N.: Properties and microstructure of a natural slip zone in loose deposits of red beds, southwestern China, Eng Geol, 183, 53-64, 10.1016/j.enggeo.2014.10.004, 2014.

Chen, S. J., Xiang, C. C., Kang, Q., Zhong, W., Zhou, Y. L., and Liu, K.: Accurate landslide detection leveraging UAV-based aerial remote sensing, Iet Commun, 14, 2434-2441, 10.1049/iet-com.2019.1115, 2020.

Chen, Z. Y., Männik, P., Fan, J. X., Wang, C. Y., Chen, Q., Sun, Z. Y., Chen, D. Y., and Li, C.: Age of the Silurian Lower
390 Red Beds in South China: Stratigraphical Evidence from the Sanbaiti Section, J Earth Sci-China, 32, 524-533, 10.1007/s12583-020-1350-6, 2021.

Ciftci, E., Hogan, J. P., Kolayli, H., and Cadirli, E.: Natrolitite, an unusual rock - Occurrence and petrographic and geochemical characteristics (eastern Turkey), Clay Clay Miner, 56, 207-221, 10.1346/Ccmn.2008.0560206, 2008.

Contino, A., Bova, P., Esposito, G., Giuffre, I., and Monteleone, S.: Historical analysis of rainfall-triggered rockfalls: the
395 case study of the disaster of the ancient hydrothermal Sclafani Spa (Madonie Mts, northern-central Sicily, Italy) in 1851, Nat Hazard Earth Sys, 17, 2229-2243, 10.5194/nhess-17-2229-2017, 2017.

Cui, G., Zhou, C., Liu, Z., Xia, C., and Zhang, L.: The synthesis of soft rocks based on physical and mechanical properties of red mudstone, International Journal of Rock Mechanics and Mining Sciences, 151, 105037, https://doi.org/10.1016/j.ijrmms.2022.105037, 2022.

400 Cunha, P., Marques, J., Curi, N., Pereira, G. T., and Lepsch, I. F.: Geomorphic surfaces and latosol (oxisol) characteristics on a sandstone/basalt sequence from the Jaboticabal region, Sao Paulo State, Brazil, Rev Bras Cienc Solo, 29, 81-90, Doi 10.1590/S0100-06832005000100009, 2005.

de Montety, V., Marc, V., Emblanch, C., Malet, J. P., Bertrand, C., Maquaire, O., and Bogaard, T. A.: Identifying the origin of groundwater and flow processes in complex landslides affecting black marls: insights from a hydrochemical survey,
405 Earth Surf Proc Land, 32, 32-48, 10.1002/esp.1370, 2007.

Feizizadeh, B., Garajeh, M. K., Blaschke, T., and Lakes, T.: An object based image analysis applied for volcanic and glacial landforms mapping in Sahand Mountain, Iran, Catena, 198, ARTN 105073 10.1016/j.catena.2020.105073, 2021.

Fu, L., Zhu, J., Li, W.-l., You, J.-g., and Hua, Z.-y.: Fast estimation method of volumes of landslide deposit by the 3D reconstruction of smartphone images, Landslides, 18, 3269-3278, 10.1007/s10346-021-01702-9, 2021.

Gao, F., Wu, X., and Deng, R.: The distribution of red beds and analysis on engineering characteristics of mudstone in Guangxi, Journal of Geological Hazards and Environment Preservation, 28, 48-52, 2017.

Garajeh, M. K., Feizizadeh, B., Blaschke, T., and Lakes, T.: Detecting and mapping karst landforms using object-based image analysis: Case study: Takht-Soleiman and Parava Mountains, Iran, The Egyptian Journal of Remote Sensing and Space Science, 25, 473-489, https://doi.org/10.1016/j.ejrs.2022.03.009, 2022.

Gokbulak, F. and Ozcan, M.: Hydro-physical properties of soils developed from different parent materials, Geoderma, 145, 376-380, 10.1016/j.geoderma.2008.04.006, 2008.

Hale, S., Ries, X., Jaeggi, D., and Blum, P.: Mechanical and hydraulic properties of the excavation damaged zone (EDZ) in the Opalinus Clay of the Mont Terri rock laboratory, Switzerland, Solid Earth, 12, 1581-1600, 10.5194/se-12-1581-2021, 2021.

Harp, E. L., Dart, R. L., and Reichenbach, P.: Rock fall simulation at Timpanogos Cave National Monument, American Fork Canyon, Utah, USA, Landslides, 8, 373-379, 10.1007/s10346-010-0251-7, 2011.

He, J., Niu, F., Luo, F., Jiang, H., He, P., and Ju, X.: Mechanical properties and modified binary-medium constitutive model for red-bed soft rock subjected to freeze-thaw cycles, Cold Reg Sci Technol, 209, 10.1016/j.coldregions.2023.103803, 2023.

He, K., Ma, G. T., and Hu, X. W.: Formation mechanisms and evolution model of the tectonic-related ancient giant basalt landslide in Yanyuan County, China, Nat Hazards, 106, 2575-2597, 10.1007/s11069-021-04555-6, 2021.

Hong, H., Li, Z., and Xiao, P.: Clay Mineralogy Along the Laterite Profile in Hubei, South China: Mineral Evolution and Evidence for Eolian Origin, Clay Clay Miner, 57, 602-615, 10.1346/Ccmn.2009.0570508, 2009.

430   Hu, X., Wang, C., Li, X., and Luba, J.: Upper Cretaceous oceanic red beds in southern Tibet: Lithofacies, environments and colour origin, Sci China Ser D, 49, 785-795, 10.1007/s11430-006-0785-7, 2006.

Jian, W. X., Wang, Z. J., and Yin, K. L.: Mechanism of the Anlesi landslide in the Three Gorges Reservoir, China, Eng Geol, 108, 86-95, 10.1016/j.enggeo.2009.06.017, 2009.

Jiang, H., Xia, Y., Li, J., Liu, S., Zhang, M., and Wang, Y.: Controlling the Iron Migration Mechanism for the Cretaceous
435   Sediment Color Variations in Sichuan Basin, China, Acs Omega, 7, 480-495, 10.1021/acsomega.1c04893, 2022.

Kavvadas, M., Roumpos, C., and Schilizzi, P.: Stability of Deep Excavation Slopes in Continuous Surface Lignite Mining Systems, Geotechnical and Geological Engineering, 38, 791-812, 10.1007/s10706-019-01066-x, 2020.

Kirsch, M., Lorenz, S., Zimmermann, R., Tusa, L., Mockel, R., Hodl, P., Booysen, R., Khodadadzadeh, M., and Gloaguen, R.: Integration of Terrestrial and Drone-Borne Hyperspectral and Photogrammetric Sensing Methods for Exploration
440   Mapping and Mining Monitoring, Remote Sens-Basel, 10, 10.3390/rs10091366, 2018.

Kong, L. W., Zeng, Z. X., Bai, W., and Wang, M.: Engineering geological properties of weathered swelling mudstones and their effects on the landslides occurrence in the Yanji section of the Jilin-Hunchun high-speed railway, B Eng Geol Environ, 77, 1491-1503, 10.1007/s10064-017-1096-2, 2018.

Li, A., Deng, H., Zhang, H., Liu, H., and Jiang, M.: The shear-creep behavior of the weak interlayer mudstone in a red-bed
445   soft rock in acidic environments and its modeling with an improved Burgers model, Mech Time-Depend Mat, 27, 1-18, 10.1007/s11043-021-09523-y, 2023.

Li, J., Xu, Q., Hu, Z., Liu, H., Zhang, Q., Lu, Y., and Wang, S.: Experimental research on softening of undisturbed saturated slip soil in eastern of Sichuan province red bed, Chinese Journal of Rock Mechanics and Engineering, 34, 4333-4342, 2015.

450   Li, S., Chen, J., and Yi, G.: Experimental study on the relationship between micro-characteristics and compressive strength of the red bed rock, Geotechnical Investigation and Surveying, 41, 1-5, 2013.

Li, X. N., Zhu, B. L., and Wu, X. Y.: Swelling characteristics of soils derived from black shales heightened by cations in Northern Chongqing, China, J Mt Sci-Engl, 13, 1107-1119, 10.1007/s11629-015-3576-9, 2016.

Liu, C., He, C., and He, M.: Engineering geology study on failure of red beds slopes along railway in the west of Hunan Province, The Chinese Journal of Geological Hazard and Control, 18, 58-62, 2007.

Liu, J., Wei, J. H., Hu, H., Wu, J. M., Sun, S. R., and Kanungo, D. P.: Research on the engineering geological conditions and stability evaluation of the B2 talus slide at the Jin'an Bridge hydropower station, China, B Eng Geol Environ, 77, 105-125, 10.1007/s10064-017-1005-8, 2018.

Liu, J., Xu, Q., Wang, S., Siva Subramanian, S., Wang, L., and Qi, X.: Formation and chemo-mechanical characteristics of weak clay interlayers between alternative mudstone and sandstone sequence of gently inclined landslides in Nanjiang, SW China, B Eng Geol Environ, 79, 4701-4715, 10.1007/s10064-020-01859-y, 2020.

Liu, X., Zhao, M., Su, Y., and Long, Y.: Grey Correlation Analysis of Slake Durability of Red Bed Weak Rock, Journal of Hunan University (Natural Sciences), 33, 16-20, 2006.

Marat, A. R., Tamas, T., Samsudean, C., and Gheorghiu, R.: Physico-mechanical and mineralogical investigations of red bed slopes (Cluj-Napoca, Romania), B Eng Geol Environ, 81, ARTN 78

10.1007/s10064-021-02542-6, 2022.

Migon, P., Woo, K. S., and Kasprzak, M.: Landform Recognition in Granite Mountains in East Asia (Seoraksan, Republic of Korea, and Huangshan and Sanqingshan, China) - a Contribution of Geomorphology to the Unesco World Heritage, Quaest Geogr, 37, 103-114, 10.2478/quageo-2018-0008, 2018.

Moonjun, R., Shrestha, D. P., Jetten, V. G., and van Ruitenbeek, F. J. A.: Application of airborne gamma-ray imagery to assist soil survey: A case study from Thailand, Geoderma, 289, 196-212, 10.1016/j.geoderma.2016.10.035, 2017.

Nance, H. S.: Interfingering of evaporites and red beds: an example from the queen/grayburg formation, Texas, Sediment Geol, 56, 357-381, 2015.

Ni, L. T., Zhong, J. H., Shao, Z. F., Li, Y., Mao, C., and Liu, S. X.: Characteristics, Genesis, and Sedimentary Environment of Duplex-Like Structures in the Jurassic Sediments of Western Qaidam Basin, China, J Earth Sci-China, 26, 677-689, 10.1007/s12583-015-0578-2, 2015.

Perez-Rey, I., Riquelme, A., Gonzalez-deSantos, L. M., Estevez-Ventosa, X., Tomas, R., and Alejano, L. R.: A multi-approach rockfall hazard assessment on a weathered granite natural rock slope, Landslides, 16, 2005-2015, 10.1007/s10346-019-01208-5, 2019.

480   Perri, F., Critelli, S., Martín-Algarra, A., Martín-Martín, M., Perrone, V., Mongelli, G., and Zattin, M.: Triassic redbeds in the Malaguide Complex (Betic Cordillera - Spain): Petrography, geochemistry and geodynamic implications, Earth-Sci. Rev., 117, 1-28, 10.1016/j.earscirev.2012.11.002, 2013.

Rainoldi, A. L., Franchini, M., Beaufort, D., Mozley, P., Giusiano, A., Nora, C., Patrier, P., Impiccini, A., and Pons, J.: Mineral reactions associated with hydrocarbon paleomigration in the Huincul High, Neuquen Basin, Argentina, Geol

485   Soc Am Bull, 127, 1711-1729, 10.1130/B31201.1, 2015.

San, N. E., Topal, T., and Akin, M. K.: Rockfall Hazard Assessment Around Ankara Citadel (Turkey) Using Rockfall Analyses and Hazard Rating System, Geotechnical and Geological Engineering, 38, 3831-3851, 10.1007/s10706-020-01261-1, 2020.

Triantafyllou, A., Mattielli, N., Clerbois, S., Da Silva, A. C., Kaskes, P., Claeys, P., Devleeschouwer, X., and Brkojewitsch,

490   G.: Optimizing multiple non-invasive techniques (PXRF, pMS, IA) to characterize coarse-grained igneous rocks used as building stones, J Archaeol Sci, 129, 10.1016/j.jas.2021.105376, 2021.

Uchida, E., Ogawa, Y., Maeda, N., and Nakagawa, T.: Deterioration of stone materials in the Angkor monuments, Cambodia, Eng Geol, 55, 101-112, Doi 10.1016/S0013-7952(99)00110-6, 2000.

Underwood, S. J., Schultz, M. D., Berti, M., Gregoretti, C., Simoni, A., Mote, T. L., and Saylor, A. M.: Atmospheric

495   circulation patterns, cloud-to-ground lightning, and locally intense convective rainfall associated with debris flow initiation in the Dolomite Alps of northeastern Italy, Nat Hazard Earth Sys, 16, 509-528, 10.5194/nhess-16-509-2016, 2016.

Wang, D., Li, X.-b., Peng, K., Ma, C., Zhang, Z., and Liu, X.: Geotechnical characterization of red shale and its indication for ground control in deep underground mining, J Cent South Univ, 25, 2979-2991, 10.1007/s11771-018-3968-4, 2018.

500   Wang, F. W., Chen, Y., Peng, X. L., Zhu, G. L., Yan, K. M., and Ye, Z. H.: The fault-controlled Chengtian landslide triggered by rainfall on 20 May 2021 in Songyang County, Zhejiang Province, China, Landslides, 19, 1751-1765, 10.1007/s10346-022-01891-x, 2022a.

Wang, L., Wang, L., Zhang, W., Meng, X., Liu, S., and Zhu, C.: Time series prediction of reservoir bank landslide failure probability considering the spatial variability of soil properties, J Rock Mech Geotech, 505   https://doi.org/10.1016/j.jrmge.2023.11.040, 2024.

Wang, M., Qi, Y. A., Li, D., Dai, M. Y., and Chang, Y. G.: Ichnofabrics and Their Environmental Interpretation from the Fluvial Deposits of the Middle Triassic Youfangzhuang Formation in Western Henan, Central China, J Earth Sci-China, 25, 648-661, 10.1007/s12583-014-0454-2, 2014.

Wang, Y., Liu, J., Yan, S., Yu, L., and Yin, K.: Estimation of probability distribution of shear strength of slip zone soils in 510   Middle Jurassic red beds in Wanzhou of China, Landslides, 14, 2165-2174, 10.1007/s10346-017-0890-z, 2017.

Wang, Y., Tang, H., Huang, J., Wen, T., Ma, J., and Zhang, J.: A comparative study of different machine learning methods for reservoir landslide displacement prediction, Eng Geol, 298, 106544, https://doi.org/10.1016/j.enggeo.2022.106544, 2022b.

Wankmuller, C., Kunovjanek, M., and Mayrgundter, S.: Drones in emergency response-evidence from cross-border, multi-515   disciplinary usability tests, Int J Disast Risk Re, 65, 10.1016/j.ijdrr.2021.102567, 2021.

Wild, K. M., Walter, P., and Amann, F.: The response of Opalinus Clay when exposed to cyclic relative humidity variations, Solid Earth, 8, 351-360, 10.5194/se-8-351-2017, 2017.

Wu, L. Z., Zhang, L. M., Zhou, Y., Xu, Q., Yu, B., Liu, G. G., and Bai, L. Y.: Theoretical analysis and model test for rainfall-induced shallow landslides in the red-bed area of Sichuan, Bulletin of Engineering Geology and the 520   Environment, 77, 1343-1353, 10.1007/s10064-017-1126-0, 2018.

Xia, K. Z., Chen, C. X., Zheng, Y., Zhang, H. N., Liu, X. M., Deng, Y. Y., and Yang, K. Y.: Engineering geology and ground collapse mechanism in the Chengchao Iron-ore Mine in China, Eng Geol, 249, 129-147, 10.1016/j.enggeo.2018.12.028, 2019.

Xue, Y., Wang, Q., Ma, L., Yu, Y., and Zhang, R.: Mechanisms and controlling factors of heave in summer for high-speed railway cutting: A case study of Northwest China, Construction and Building Materials, 365, 10.1016/j.conbuildmat.2022.130061, 2023.

Yan, L. B., Peng, H., Zhang, S. Y., Zhang, R. X., Kasanin-Grubin, M., Lin, K. R., and Tu, X. J.: The Spatial Patterns of Red Beds and Danxia Landforms: Implication for the formation factors-China, Sci Rep-Uk, 9, 10.1038/s41598-018-37238-7, 2019.

Yang, Y., Zhou, J., Xu, F., and Xing, H.: An Experimental Study on the Water-Induced Strength Reduction in Zigong Argillaceous Siltstone with Different Degree of Weathering, Adv Mater Sci Eng, 10.1155/2016/4956986, 2016.

Yao, H., Jia, S., Gan, W., Zhang, Z., and Lu, K.: Properties of Crushed Red-Bed Soft Rock Mixtures Used in Subgrade, Adv Mater Sci Eng, 2016, 10.1155/2016/9624974, 2016.

Zha, F., Huang, K., Kang, B., Sun, X., Su, J., Li, Y., and Lu, Z.: Deterioration Characteristic and Constitutive Model of Red-Bed Argillaceous Siltstone Subjected to Drying-Wetting Cycles, Lithosphere-Us, 2022, 8786210, 10.2113/2022/8786210, 2022.

Zhang, M., Yin, Y., and Huang, B.: Mechanisms of rainfall-induced landslides in gently inclined red beds in the eastern Sichuan Basin, SW China, Landslides, 12, 973-983, 10.1007/s10346-015-0611-4, 2015.

Zhang, S., Xu, Q., and Hu, Z. M.: Effects of rainwater softening on red mudstone of deep-seated landslide, Southwest China, Eng Geol, 204, 1-13, 10.1016/j.enggeo.2016.01.013, 2016.

Zhang, W., Lin, S., Wang, L., Wang, L., Jiang, X., and Wang, S.: A novel creep contact model for rock and its implement in discrete element simulation, Comput Geotech, 167, 106054, https://doi.org/10.1016/j.compgeo.2023.106054, 2024.

Zhang, Y., Li, F., and Chen, J.: Analysis of the interaction between mudstone and water, Journal of Engineering Geology, 16, 22-26, 2008.

Zhang, Z., Gao, W., Zeng, C., Tang, X., and Wu, J.: Evolution of the disintegration breakage of red-bed soft rock using a logistic regression model, Transp Geotech, 24, 10.1016/j.trgeo.2020.100382, 2020.

Zhang, Z. H., Chen, X. C., Yao, H. Y., Huang, X., and Chen, L. W.: Experimental Investigation on Tensile Strength of Jurassic Red-Bed Sandstone under the Conditions of Water Pressures and Wet-Dry Cycles, Ksce J Civ Eng, 25, 2713-2724, 10.1007/s12205-021-1404-z, 2021.

550 Zhang, Z. L., Wang, T., Wu, S. R., Tang, H. M., and Liang, C. Y.: The role of seismic triggering in a deep-seated mudstone landslide, China: Historical reconstruction and mechanism analysis, Eng Geol, 226, 122-135, 10.1016/j.enggeo.2017.06.001, 2017.

Zhao, M., Liu, X., and Su, Y.: Experimental studies on engineering properties of red bed material containing slaking rock, Chinese Journal of Geotechnical Engineering, 27, 667-671, 2005.

555 Zhou, C., Hu, Y., Xiao, T., Ou, Q., and Wang, L.: Analytical model for reinforcement effect and load transfer of pre-stressed anchor cable with bore deviation, Construction and Building Materials, 379, 131219, https://doi.org/10.1016/j.conbuildmat.2023.131219, 2023a.

Zhou, C., Yu, L., Huang, Z., Liu, Z., and Zhang, L.: Analysis of microstructure and spatially dependent permeability of soft soil during consolidation deformation, Soils Found, 61, 708-733, https://doi.org/10.1016/j.sandf.2021.02.004, 2021.

560 Zhou, C., Liu, Z., Xue, Y., Li, Y., Fan, X., Chen, W., and Sun, P.: Some thoughts on basic research of red beds disaste, Journal of Engineering Geology, 31, 689-705, 10.13544/j.cnki.jeg.2022-0842, 2023b.

Zhu, B., Hu, H., and Chen, Q.: Preliminary study on the characteristics and hazards of M - shaped roadcut slope in red beds, Journal of Engineering Geology, 11, 411-415, 2003.